npj | climate and atmospheric science

www.nature.com/npjclimatsci

ARTICLE OPEN

Check for updates

Elucidating HONO formation mechanism and its essential contribution to OH during haze events

Xinran Zhang[1,2], Shengrui Tong[1]✉, Chenhui Jia[1], Wenqian Zhang[1], Zhen Wang[1], Guiqian Tang[3], Bo Hu[3], Zirui Liu[3], Lili Wang[3], Pusheng Zhao[4,5], Yuepeng Pan[3] and Maofa Ge[1,2]✉

Atmospheric nitrous acid (HONO) chemistry is of critical importance to air quality during polluted haze events, especially in China. However, current air quality models (such as WRF-CHEM, WRF-CMAQ, Box-MCM) generally underestimate the concentration of HONO, leading to a lack of fundamental understanding of haze pollution. Here, by combining field observations during haze events in Beijing and modeling results, we developed the new parameterization scheme for heterogeneous nitrogen dioxide (NO_2) reaction on aerosol surfaces with the synergistic effects of relative humidity and ammonia, which has not been considered in existing air quality models. Including NO_2 heterogeneous reactions into modeling significantly improves the estimation accuracy of HONO and OH levels, with the contribution reaching up to 91% and 78% during pollution episodes. The OH derived by HONO can partly explain high concentrations of particulate matter. Together, our work provides a new approach to illustrate the formation of HONO, OH, and haze with the consideration of heterogeneous $NO_2 \rightarrow$ HONO chemistry.

npj Climate and Atmospheric Science (2023)6:55 ; https://doi.org/10.1038/s41612-023-00371-w

INTRODUCTION

The World Health Organization (WHO) reports that air pollution leads to several million premature deaths a year[1]. The main culprit, haze pollution, is a global issue and brings a wide range of negative health impacts (such as cancer, respiratory and heart diseases) to human body[2–5]. Nowadays, particle pollution risks still occur in developed countries[6,7] and are urgent in developing countries[5,8,9]. Previous study has proposed that up to 77% $PM_{2.5}$ (particulate matter with an aerodynamic diameter less than 2.5 μm) was contributed by secondary aerosol formation[5]. Therefore, understanding the main drivers (atmospheric oxidants and oxidation pathways) for secondary aerosol formation is of significance for figuring out haze pollution[10,11].

As part of the haze production, nitrous acid (HONO) photolysis contributes to more than 50% of hydroxyl radical (OH), which strongly impact the atmospheric oxidation capacity[12–14]. In the case of the North China Plain, the more serious the pollution, the greater the contribution from HONO to OH (the contribution reached up to 93% during heavily polluted episodes)[15]. The OH levels contributed by HONO facilitates the secondary processes during haze pollution. Therefore, HONO is the underlying controlling factor of haze, especially under severe polluted periods[16,17].

Generally, models underestimate HONO, which impacts OH predictions and ultimately secondary aerosol formation (especially in highly populated regions)[15,18,19]. In model simulations, the most common HONO source is homogeneous reaction of OH and nitric oxide (NO)[20,21]. It is also known that HONO sources include direct emissions[22–24], heterogeneous reactions of nitrogen dioxide (NO_2) on wet surfaces[25–27], photo-enhanced NO_2 heterogeneous conversion[28], and photolysis of atmospheric NO_3^- and surface adsorbed nitric acid (HNO_3)[29–32], etc. Also, there were some influencing factors for HONO formation mechanisms such as RH-promoted NO_2 heterogeneous conversion[33,34], NH_3-promoted NO_2 hydrolysis[35], oxidation of SO_2 by NO_2[36], etc. Even though some model simulations could well simulate HONO observations, they use the single NO_2 uptake coefficient to measure NO_2 hydrolysis and not considered any known influencing factors such as RH[15,18]. Previous studies have proposed the parameterization of RH factor to NO_2 heterogeneous conversion, but there is still a big difference with the observed HONO[37,38]. At present, the controversy for HONO formation focused on the quantification and parameterization scheme of NO_2 heterogeneous reactions (the dominant source during nighttime and polluted days[39]). Indeed, despite the progress in the development of HONO formation mechanisms, a HONO model parameterization scheme that can be widely used to accurately predict HONO concentration remains elusive.

Here, the atmospheric concentrations of HONO and related species were simultaneously measured in urban Beijing, from October 25 to December 7, 2018. We developed the new parameterization scheme of NO_2 conversion to HONO. Via observation-based box modeling involving Master Chemical Mechanism (MCM v3.3.1) simulations, we test the HONO parameterization scheme out for Beijing and it works very well. The more accurate HONO quantification here can help to accurately estimate OH and ultimately haze formation, which has implications for global and regional models everywhere.

RESULTS AND DISCUSSION

Field observations and HONO variation characteristics

Continuous measurements of HONO and related species (including environmental parameters, gaseous species, particle constituents, photolysis frequencies, volatile organic compounds, etc) were conducted in wintertime Beijing, from October 25 to December 7,

[1]State Key Laboratory for Structural Chemistry of Unstable and Stable Species, CAS Research/Education Center for Excellence in Molecular Sciences, Institute of Chemistry, Chinese Academy of Sciences, 100190 Beijing, P. R. China. [2]University of Chinese Academy of Sciences, 100049 Beijing, P. R. China. [3]State Key Laboratory of Atmospheric Boundary Layer Physics and Atmospheric Chemistry (LAPC), Institute of Atmospheric Physics (IAP), Chinese Academy of Sciences, 100029 Beijing, P. R. China. [4]Joint laboratory for electron microscopy analysis of atmospheric particles, 100012 Beijing, China. [5]Institute of Urban Meteorology, China Meteorological Administration, 100089 Beijing, P. R. China. ✉email: tongsr@iccas.ac.cn; gemaofa@iccas.ac.cn

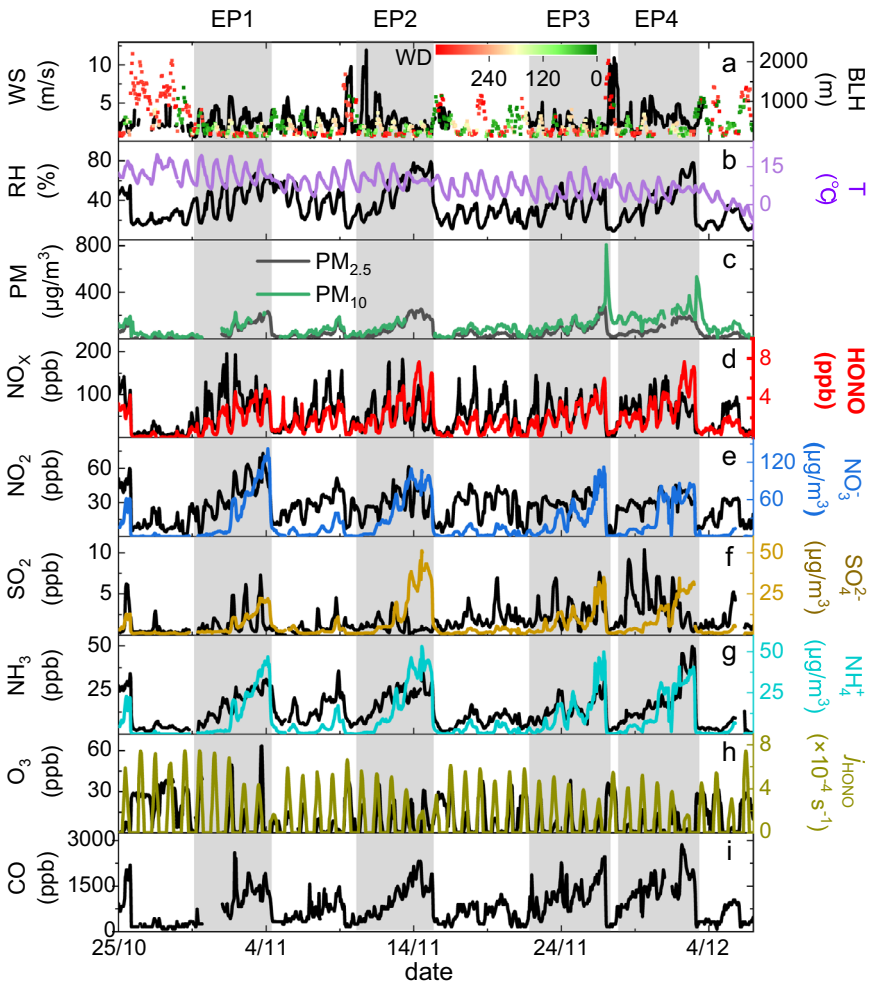

Fig. 1 Time series (local time) of meteorology parameters and chemical species from October 25 to December 7, 2018 in Beijing. a Wind speed (WS) colored by wind direction (WD) and boundary layer height (BLH) above ground level. **b** Relative humidity (RH) and temperature (T). **c** $PM_{2.5}$ and PM_{10} concentrations. **d** NO_X ($NO + NO_2$) and HONO concentrations. **e** NO_2 and $PM_{2.5}$ nitrate (NO_3^-) concentrations. **f** SO_2 and $PM_{2.5}$ sulfate (SO_4^{2-}) concentrations. **g** NH_3 and $PM_{2.5}$ ammonium (NH_4^+) concentrations. **h** O_3 and j_{HONO} concentrations. **i** CO concentrations. The gray shaded areas are four pollution episodes, named PE1, PE2, PE3, PE4.

2018. The variation of meteorological parameters and chemical species concentrations during field observation period is illustrated in Fig. 1. The observed average mass concentration of $PM_{2.5}$ and PM_{10} were 63 ± 63 μg/m^3 and 102 ± 84 μg/m^3, with maximum values of 275 μg/m^3 and 810 μg/m^3, respectively. Due to the occurrence of dust storms, the PM_{10} concentration was >320 μg/m^3 on November 27 (00:00–06:00) and December 3 (03:00–10:00), along with high wind speed (WS), high boundary layer height (BLH), and low RH conditions. To exclude the impact of dust storms, the analysis is focused on non-storm period. During the field observation period, four pollution episodes occurred as shown in the shadow regions in Fig. 1 and Supplementary Table 3, i.e., pollution episode (PE) 1–4. Before each pollution episode, there was a gust of wind (higher than 2 m/s) from the northwest and the northeast, carrying relatively clean air masses from the less populated northern mountainous areas. During the four episodes, low wind speed (WS < 2 m/s) led to more stable meteorological dispersion conditions, with a higher RH and lower BLH compared to unpolluted periods[40,41]. The $PM_{2.5}$ properties showed a typical periodic cycle within 4–7days[42], with mass concentrations <30 μg/m^3 at the beginning of each cycle, then developing to up to 275 μg/m^3 within 2–5 days[40]. Each individual pollution episode had three successive days that exceeded the China National Ambient Air Quality Standard (CNAAQS, 75 μg/m^3 for a 24 h average). RH exhibited a similar tendency with $PM_{2.5}$. The average $PM_{2.5}$ concentration and RH in four pollution episodes were 102 ± 71 μg/m^3 and 43 ± 14%, 115 ± 81 μg/m^3 and 50 ± 18%, 89 ± 62 μg/m^3 and 35 ± 11%, and 95 ± 56 μg/m^3 and 41 ± 17%, respectively. These four selected pollution episodes were representative of typical periodic haze pollution cycles in urban China, which were associated with stagnant meteorological conditions such as low air diffusion rates and high humidity[40,43]. Analysis on these pollution episodes provides important insights into the HONO formation mechanism in Beijing haze, as discussed below.

In each pollution episode, the concentrations of HONO, NO_2, CO, and NH_3 showed a gradual increase with increased concentration of $PM_{2.5}$ compositions (e.g., NH_4^+, SO_4^{2-}, NO_3^-), implying the potential link between these gaseous species and the formed $PM_{2.5}$[44]. SO_2 increased with SO_4^{2-} developed in PE1 but decreased with SO_4^{2-} developed at the end stages of PE2 and PE4 (suggesting the fast conversion of SO_2 to SO_4^{2-}). O_3 concentration generally stayed at a low level due to the weak photochemical reactivity during haze pollution, and possessed a negative relationship with $PM_{2.5}$ concentration. The highest O_3 concentration was observed in PE1 (daytime (8:00−16:00) average value was 18 ± 15 ppb), together with the highest HONO photolysis frequency (j_{HONO}, daytime average value was $(4.3 \pm 1.7) \times 10^{-4}$ s^{-1}), which reflected the highest solar radiation

among four episodes. NO_X ($NO + NO_2$, the major precursor of HONO) showed similar variation trends with HONO. The diurnal variation profile of HONO, NO, and NO_2 are summarized in Supplementary Fig. 1, similar to those reported by previous haze studies[45–47]. Specifically, daytime photoreactions and lifted BLH lead to low diurnal concentrations of HONO with the minimum value at noon (around 15:00). After sunset, BLH gradually declined and pollutants accumulated until the early morning, resulting in high HONO concentrations during nighttime. The observed HONO concentrations were higher in PE2 (2.83 ± 1.84 ppb) and PE4 (3.04 ± 1.71 ppb) compared to PE1 and PE3, especially at midnight and in the early morning. However, higher NO and NO_2 values were observed in PE1 (38.06 ± 35.12 ppb, 35.82 ± 15.97 ppb) and PE4 (38.71 ± 24.42 ppb, 30.98 ± 6.48 ppb) compared to PE2 and PE3. Nocturnal NO concentrations were sometimes higher than NO_2, which revealed the importance of freshly released plumes. Overall, the relationship between HONO and NO_X is not straightforward, indicating that the formation of HONO is controlled by multiple factors.

The overview of daytime (8:00–16:00), nighttime (18:00–06:00), and daily mean concentrations of HONO, NO_2, NO, and $PM_{2.5}$ during four episodes investigated here and the previously reported data during winter haze events are summarized in Supplementary Table 4. During the four pollution episodes, the average values of HONO, NO, NO_2, and $PM_{2.5}$ were 2.52 ± 1.61 ppb, 35.14 ± 30.27 ppb, 32.23 ± 7.43 ppb, 100 ± 69 μg/m^3, respectively, which were at an intermediate level compared with previous studies in China[48–50] and other countries such as India[8,9]. The ratio of HONO to NO_X (i.e., the conversion frequency from NO_X to HONO), was around 0.03 among previously reported winter haze events in China before 2018[15,45–47,51]. In this study, the average HONO/NO_X value was 0.039 ± 0.021, implying a higher NO_X to HONO conversion frequency level in recent years.

The net homogeneous reaction rate (P_{net}, including the reactions of OH with NO and OH with HONO as shown in Supplementary Note 3) in four episodes during 11:00–14:00 were 0.66 ppb/h, which was about 40% higher than the previous observations[48,52]. The daily average NO concentrations in four episodes were above 29 ppb. Recent studies also reported high NO concentrations in China[48,51]. Therefore, the homogeneous source ($OH + NO \rightarrow HONO$) may play an important role in the formation of HONO. Vehicle emission is the most important direct emission source of HONO in urban areas[53,54]. As shown in Supplementary Fig. 2, the correlation coefficient (R^2) between HONO and NO_X was 0.61 in PE1, followed by 0.56 in PE3, 0.40 in PE2, and 0.29 in PE4. We note that when HONO concentrations are below 3 ppb, the R^2 between HONO and NO_X increased to 0.81, 0.42, 0.38, and 0.35 for PE 1–4, respectively. However, for more polluted periods during which HONO concentration was higher than 3 ppb, no significant correlation was found between HONO and NO_X. As shown in Supplementary Note 2, HONO emission factor inferred by the ratio of HONO to NO_X emissions was 0.00973. Direct emission factor can be corrected by multiplying the ratio of the τ(HONO)/τ(NO_X) (HONO lifetime/NO_X lifetime) when τ(HONO) was less than 1h[55]. Contributions of vehicle emitted HONO to total observed HONO ($HONO_{emission}$/HONO) was higher in PE1 (28%) and PE3 (27%), followed by PE4 (21%), and PE2 (18%). The peaks of $HONO_{emission}$/HONO usually appeared in morning rushing hours (around 08:00) and evening rushing hours (around 22:00). $HONO_{emission}$/HONO was larger during periods with lower-level HONO concentrations, which corresponded to lower-level $PM_{2.5}$ concentrations. The results implied that the contribution of vehicle emission to HONO was more significant on less polluted days, while was less important on more polluted days (i.e., with higher $PM_{2.5}$ concentration). The heterogeneous NO_2 conversion fraction ($HONO_{corr}/NO_2$, $HONO_{corr} = HONO - HONO_{emission}$) was used to evaluate the impact of heterogeneous NO_2 conversion. As shown in Supplementary Fig. 4, $HONO_{corr}/NO_2$ in PE2 (7.6%) and PE4 (7.6%) were higher than those in PE1 (3.5%) and PE3 (5.0%), implying the potential stronger capacity of heterogeneous conversion from NO_2 to HONO in PE2 and PE4. In theory, the $NO_2 \rightarrow HONO$ conversion can take place on both aerosol surface and ground surface. The positive correlation of $HONO_{corr}$ with NO_2, $PM_{2.5}$, and $NO_2 \times PM_{2.5}$ in Supplementary Fig. 5 demonstrated that NO_2 heterogeneous reactions on $PM_{2.5}$ surfaces were important, especially in PE2 and PE4. Other NO_2 heterogeneous pathways may also influence HONO production when RH is higher than 70%. As shown in Supplementary Fig. 6 and Supplementary Discussion, higher RH (>70%) and $PM_{2.5}$ (>150 μg/m^3) in PEs could accelerate NO_2 heterogeneous conversion, the corresponding episodes were denoted as SPEs (severe pollution episodes).

Model simulations and unknown HONO sources

The box model simulations with Master Chemical Mechanism, MCM v3.3.1 mechanisms were used to reveal the relative importance of different HONO sources in urban Beijing. The base HONO source in model simulations includes homogeneous OH + NO reaction, and the base HONO loss pathways include HONO photolysis, OH + HONO reaction, and HONO deposition[51,56,57]. The base model ($HONO_{base}$) can only explain 8% of observed HONO in PEs (Supplementary Fig. 7), which can further underestimate OH and O_3 in the atmosphere[18,58]. Therefore, we considered other known HONO formation mechanisms (including NO_2 heterogeneous reaction on the ground surface and photo-enhanced NO_2 heterogeneous reaction on the ground surface ($HONO_{ground}$, ppb), NO_2 heterogeneous reaction on the aerosol surface and photo-enhanced NO_2 heterogeneous reaction on the aerosol surface ($HONO_{aerosol}$, ppb), surface adsorbed HNO_3 photolysis ($HONO_{HNO3}$, ppb), atmospheric NO_3^- photolysis ($HONO_{NO3-}$, ppb), and $HONO_{emission}$) in the box model simulations (Table 1). Table 1 represents a general consideration for HONO sources parameterization scheme. After including these HONO sources in model simulations, the simulated HONO concentrations ($HONO_{sim}$, $HONO_{base} + HONO_{ground} + HONO_{aerosol} + HONO_{HNO3} + HONO_{NO3-} + HONO_{emission}$) can explain about 85% of the observed HONO in PEs but only 12% in SPEs. The unknown HONO concentrations can be shown as $HONO_{unknown}$ (observed HONO minus $HONO_{sim}$) The contribution ratio of $HONO_{unknown}$ ($HONO_{unknown}$/HONO) was 2%, 26%, 11%, and 15% in PE1–4, respectively. With $PM_{2.5}$ concentration increased in a given pollution episode, $HONO_{unknown}$/HONO also increased (Supplementary Fig. 10). Figuring out $HONO_{unknown}$ could provide a previously unrecognized oxidation pathway in the atmosphere through HONO photolysis. The unrecognized oxidation pathway can further explain the exceedingly high levels of particle concentrations, which were generally significantly underestimated in previous studies[10,11].

Through linear regression analysis for $HONO_{unknown}$ and gaseous species concentration and environmental conditions, we found that CO, NH_3, $PM_{2.5}$, and RH had good correlations with unknown HONO concentrations (Fig. 2). The black and red dots in Fig. 2 represent PEs (except SPEs) and SPEs, respectively. There was no direct connection between CO and HONO production. Due to the strong correlation between CO and $PM_{2.5}$ ($R^2 = 0.72$) and the homology of CO, NH_3, and NO_X, $HONO_{unknown}$ showed a good correlation with CO. Therefore, we focused on the effect of RH, NH_3, and $PM_{2.5}$ on HONO production. To explore the effect of RH and $PM_{2.5}$ on HONO formation, ISORROPIA-2 thermodynamic equilibrium model simulations were performed to determine aerosol liquid water content (ALWC) and aerosol pH. Generally, when RH is below 40%, ALWC is very small and the estimated aerosol pH is highly uncertain[59]. For that reason, we only analyzed the data with RH higher than 40%. The average values of ALWC in

Table 1. Parameters of HONO source/loss mechanisms in model simulations.

HONO formation/loss pathways	Rate constant and emission factor
Vehicle emissions	emission factor was 0.00973
$OH + NO \rightarrow HONO$	k was calculated in the MCM mechanism
$2NO_2 + H_2O \xrightarrow{\text{aerosol surface}} HONO + HNO_3$	$k = 0.125 \times C_{NO_2} \times S_{aero} \times \gamma_a$
$NO_2 + h\nu \xrightarrow{\text{aerosol surface}} HONO$	$k = 0.25 \times C_{NO_2} \times S_{aero} \times \gamma_{a,h\nu} \times \frac{j_{NO_2}}{0.005s^{-1}}$
$2NO_2 + H_2O \xrightarrow{\text{ground surface}} HONO + HNO_3$	$k = \frac{0.125 \times C_{NO_2} \times \gamma_g}{MLH}$
$NO_2 + h\nu \xrightarrow{\text{ground surface}} HONO$	$k = \frac{0.25 \times C_{NO_2} \times \gamma_{g,h\nu}}{MLH} \times \frac{j_{NO_2}}{0.005s^{-1}}$
$HNO_3 + h\nu \rightarrow 0.67HONO + 0.33NO_X$	$k = \frac{0.25 \times v_{HNO_3} \times t_d \times j_{HNO_3} \times 0.67}{BLH}$
$NO_3^- + h\nu \rightarrow 0.67HONO + 0.33NO_X$	$k = 0.67 \times j_{NO_3}$
$HONO + h\nu \rightarrow OH + NO$	j_{HONO}
$HONO + OH \rightarrow H_2O + NO_2$	k was calculated in the MCM mechanism
HONO deposition	$k = -\frac{v_{HONO}}{BLH}$

C_{NO2} was the mean molecular speed of NO_2. S_{aero} was the aerosol surface ($\mu m^2/cm^3$). As shown in Supplementary Note 4, γ_a and γ_g were the NO_2 uptake coefficient on the aerosol and ground surfaces, which were 2.6×10^{-5} and 1.3×10^{-6}, respectively. $\gamma_{a,h\nu}$ and $\gamma_{g,h\nu}$ were the photo-enhanced NO_2 uptake coefficient on the aerosol and ground surfaces, which were 3.9×10^{-5} and 2×10^{-6}, respectively. Photo-enhanced heterogeneous reaction factor is $\frac{j_{NO_2}}{0.005s^{-1}}$. Mixing layer height (MLH) of HONO was estimated as 50 m[55]. The average HNO_3 dry deposition velocity ($vHNO_3$) was 0.05 m/s. Assuming that the surface deposited HNO_3 is exposed to 1/4 of the full noontime sun during the day. The time interval (t_d) is one hour. Adsorbed HNO_3 photolysis rate (j_{HNO3}) of 1.2×10^{-5} was determined from the previous study[98]. However, the contribution from HNO_3 photolysis was too small to be considered. Gaseous HNO_3 photolysis rate ($j_{HNO3,\ MCM}$) is calculated from the box model simulation. Particulate NO_3- photolysis rate, $j_{NO_3} = \frac{8.3 \times 10^{-5}}{7 \times 10^{-7}} \times j_{HNO3,MCM}$. The average HONO dry deposition velocity (vHONO) was 2 cm/s[99].

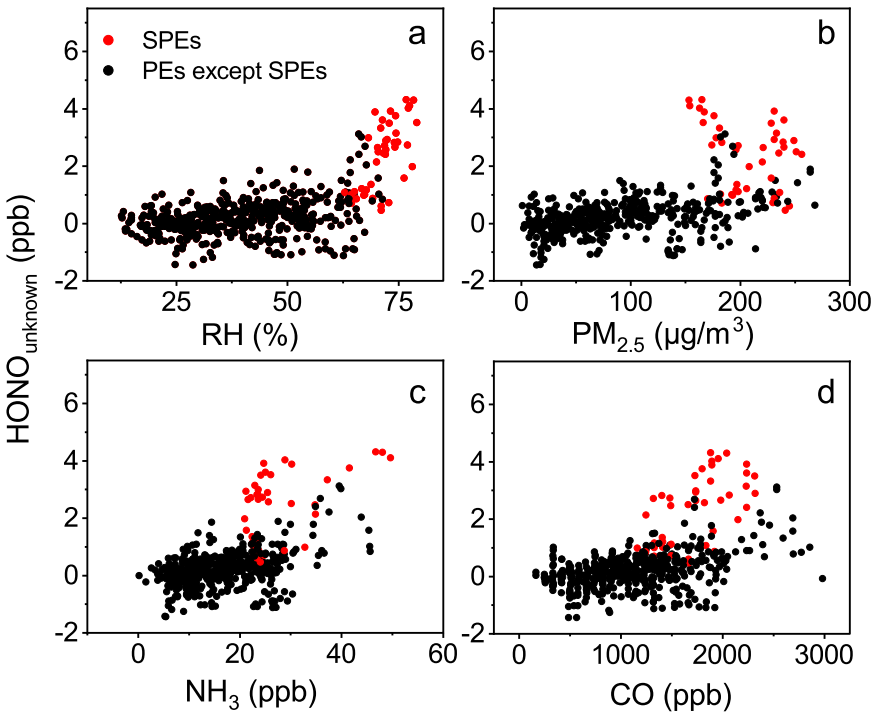

Fig. 2 Relationship between $HONO_{unknown}$ and main influencing factors in PEs. The influencing factors include (**a**) RH, (**b**) $PM_{2.5}$, (**c**) NH_3, and (**d**) CO. Red scatters are data with RH > 70% and $PM_{2.5}$ >150 μg/m^3, named SPEs.

four episodes were 40.7, 86.6, 32.5, and 59.3 μg/m^3, respectively. The average aerosol pH values in PE1–4 were 4.57, 4.39, 4.92, and 4.93, respectively, which were buffered by the conjugate acid-base pair NH_4^+/NH_3[60].

During haze events, higher RH (>40%) provides higher ALWC and improves the NO_2 uptake coefficient on aerosol surfaces[61,62]. Zheng et al.[10] proposed that the formation rate of sulfate and nitrate generated by heterogeneous reactions to form HONO increased with the increase of RH, including the NO_2 heterogeneous reaction on the aerosol surfaces. Previous study suggested that NH_3 concentrations of higher than 10 ppb would be sufficient to the new particle formation in the highly polluted atmosphere[63]. In this study, NH_3 and $HONO_{unknown}$ had clearly positive correlations when NH_3 was higher than 11 ppb (corresponded RH was higher than 40%), which indicated the effectiveness of NH_3 and RH promoted HONO formation.

Therefore, the enhanced NO_2 heterogeneous reaction on the aerosol surface under higher RH conditions may be regulated by NH_3 concentrations. Li et al. have proposed that NH_3 can promote NO_2 hydrolysis at the air-water interface to produce HONO, which may be an important process at polluted sites where NH_3 is rich[35]. The role of NH_3 is to stabilize the reaction system and promote HONO formation. Therefore, the enhanced NO_2 heterogeneous reaction on the aerosol surfaces when RH > 40% can be explained by the effect of NH_3 on the aerosol. NH_3, as an alkaline gas in the atmosphere, plays an important role in aerosol pH. High aerosol pH increases the solubility of acidic gas and thus increases the reaction rate[64,65]. Ding et al.[66] proposed a relationship between NH_3 and aerosol pH: variation of NH_3 in a low concentration range has a significant effect on aerosol pH, while the variation of NH_3 in a high concentration has little effect on aerosol pH. Hence, when RH was higher than 40%, the enhancement effect on NO_2 heterogeneous conversion on the aerosol surfaces could be expressed as $NH_3 \times k/(NH_3 + 10)$. k is the coefficient measuring the combined effect of NH_3 and RH on HONO formation. Assuming that the unexplained HONO concentrations come from the enhanced NO_2 heterogeneous conversion, we try to calculate the potential factor between unknown HONO production rate and RH, NH_3. Then, the k of 1.93 can better measure the HONO concentrations when $40\% < RH \leq 70\%$.

In SPEs, higher slopes were found between $HONO_{unknown}$ and CO, NH_3, $PM_{2.5}$, RH compared with other periods. Furthermore, the slope between $HONO_{unknown}$ and NO_2 was higher than in the other periods (Supplementary Fig. 8), suggesting a more rapid conversion rate from NO_2 to HONO. The $PM_{2.5}$ constituents have a strong hygroscopic capacity, aerosols can continuously absorb ambient water until the aerosol particles are in equilibrium with ambient air. Indeed, ALWC increased exponentially with RH (Supplementary Fig. 9)[67]. When RH is higher than 70%, $PM_{2.5}$ particles were in a deliquesced state. Based on the high gas-to-particle conversion under high RH, the NO_2 heterogeneous conversion frequency on the aerosol surfaces would be enhanced in SPEs[68,69]. NO_2 hydrolysis could be accelerated sharper when RH > 70% than that when $40\% < RH \leq 70\%$[10,37].

Additionally, the higher intercept between SO_4^{2-} and NO_3^- in SPEs relative to other periods suggested the higher conversion ratio from SO_2 to SO_4^{2-} (Supplementary Fig. 8). A recent study showed that HONO reacts with SO_2 to form SO_4^{2-} at pH values greater than 4.5 during cold winter haze days[70]. Given that the average aerosol pH in SPEs was 4.28, HONO-SO_2 chemistry is unlikely to play an important role in the formation of SO_4^{2-}. Furthermore, Liu et al.[36] have performed a series of experiments with deliquesced particles at pH values of 4–5 with experimental conditions similar to our observation conditions, which indicated that (1) SO_2 oxidation by HONO was negligible, (2) the NO_2 and SO_2 reaction at NH_3 buffered pH values of 4–5 on aerosol surfaces have atmospheric importance under haze conditions, which was mainly contributed by $NO_2 + SO_3^{2-}$ reaction, (3) the increased RH and NH_3 concentrations significantly increased NO_2 and SO_2 reaction rate. In our study, apart from the more rapid NO_2 to HONO conversion frequency and SO_2 to SO_4^{2-} conversion frequency in SPEs, there was also a change in the relationship between NO_2 and SO_4^{2-} (Supplementary Fig. 8). The increased SO_4^{2-} concentrations in SPEs may arise from the oxidation of SO_2 by NO_2 on the deliquesced aerosol particles, along with the production of HONO[36]. pH values of 4–5 were predicted for ambient aerosols during haze events by thermodynamic models[36,71,72], which was similar to the pH in SPEs.

$$2NO_2 + SO_3^{2-} + H_2O \rightarrow 2HONO + SO_4^{2-} \quad (1)$$

As shown in Supplementary Fig. 8, because NO_2 hydrolysis and $NO_2 + SO_3^{2-}$ reaction were both NO_2 heterogeneous reactions, positive correlation was found between $HONO_{unknown}$ and NO_2 in SPEs. However, SO_4^{2-}/NO_3^- was part of the NO_2 reaction product, leading to the not positively correlated relationship between SO_4^{2-}/NO_3^- and NO_2 in SPEs. Summing up, the NO_2 heterogeneous conversion (including NO_2 hydrolysis and $NO_2 + SO_3^{2-}$ reaction) should be considered in SPEs. Previous studies have suggested that the NO_2 uptake coefficient can be increased fourfold under high humidity (RH > 70%) due to the RH enhancement effects[10,37]. Additionally, NH_3 can promote NO_2 hydrolysis[35]. Previous field observations, laboratory experiments, and molecular dynamics simulations have proposed that NH_3 can accelerate NO_2 and SO_2 reaction[73–75]. The enhancement effect for NO_2 hydrolysis and $NO_2 + SO_3^{2-}$ reaction conversion rate under SPEs should be considered because: (1) the enhanced ALWC accelerated the NO_2 heterogeneous conversion to form HONO on the aerosol surface; (2) RH of higher than around 70% corresponded to the $PM_{2.5}$ particles in a deliquesced state; (3) the heterogeneous reactions of NO_2 and SO_2 on the deliquesced aerosol particles with pH values of 4–5 accelerated HONO formation. Even though the relative contribution of NO_2 and SO_2 reaction and NO_2 hydrolysis to HONO formation may be different, the inner reason was the effect of aerosol pH and deliquesced particles to increase the uptake of NO_2 on the aerosol surface. Therefore, under seriously polluted conditions (RH > 70% and $PM_{2.5}$ > 150 μg/m^3), an enhancement factor of 4 multiplied by $\frac{NH_3 \times 1.93}{NH_3 + 10}$ was used to quantify the impact of NH_3, RH on the NO_2 uptake coefficient on the aerosol surface.

Overall, according to the differences between the model results and the observations, the correlation analysis between unknown HONO and other species, and experimental and theoretical evidence from the previous studies[35,36,73,75], the enhancement factor ($f_{NH3,\ RH}$, as follows) for NO_2 uptake coefficient on the aerosol surface (divided by RH and $PM_{2.5}$ concentrations) was included in model simulations.

$$f_{NH_3,RH} = \begin{cases} 1, & RH \leq 40\% \\ \frac{NH_3 \times 1.93}{NH_3 + 10}, & 40\% < RH \leq 70\% \\ \frac{NH_3 \times 1.93}{NH_3 + 10} \times 4, & RH > 70\%, PM_{2.5} > 150 \mu g/m^3 \end{cases} \quad (2)$$

Under typical winter haze in Beijing when $40\% < RH \leq 70\%$, RH and NH_3 can promote the NO_2 hydrolysis at the air-water interface to produce HONO. As pollution developed when RH > 70%, the aerosols grew fast and ALWC dramatically increased because of the strong hygroscopic capacity of water-soluble ions. The increased ALWC and NH_3 can further increase gaseous species (such as NO_2) uptake and increase gas-to-particle conversion, which derived both NO_2 hydrolysis and NO_2 heterogeneous conversion with SO_3^{2-} at aerosol pH 4–5. By increasing the NO_2 uptake coefficient on the aerosol surface by the factor of $f_{NH3,\ RH}$ without adjustment, model performance on HONO simulations in PE1–4 was nearly approach to the level of observed HONO (Supplementary Fig. 10). In PE1–4, the final simulated HONO explained observed HONO of about 107%, 97%, 94%, and 97%, respectively. $f_{NH3,\ RH}$ explained HONO of about 13% in PEs (41% in SPEs). $f_{NH3,\ RH}$ had a small impact on the period with RH ≤ 70%, but a large impact on the SPEs period. $f_{NH3,\ RH}$ was an important factor to measure the HONO concentrations during severe polluted episodes.

In PEs, the contributions of sources to HONO formation are expressed in Fig. 3 and Supplementary Table 6. The base model with only one HONO production pathway of homogeneous reaction of NO and OH can contribute to 12% diurnal HONO and 6% nocturnal HONO. In urban sites with large NO_X emissions, vehicle emissions were always a considerable nocturnal HONO source. The contribution from the photolysis of nitrate to diurnal HONO formation was about 2% during haze events. The photolysis of HNO_3 and NO_3^- was negligible to HONO formation. Ye[31] proposed that j_{NO3} (s^{-1}) varies from 6.2×10^{-6} to 5×10^{-4}.

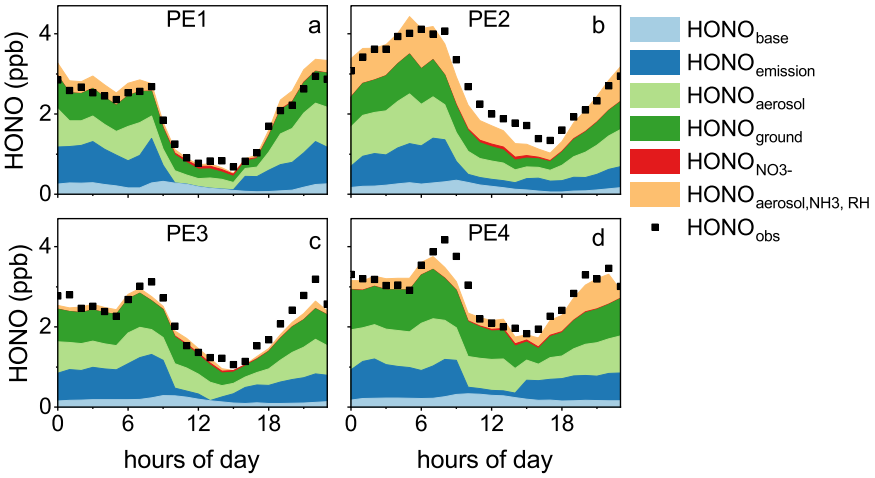

Fig. 3 Diurnal variations of the HONO sources during four pollution episodes. In (**a**) PE1, (**b**) PE2, (**c**) PE3, and (**d**) PE4, the light blue area represents the base model simulation ($HONO_{base}$). The added HONO sources were the dark blue area (HONO concentrations from vehicle emission, $HONO_{emission}$), light green area (HONO concentrations from NO_2 heterogeneous reaction on the aerosol surface and photo-ienhanced mechanisms, $HONO_{aerosol}$), dark green area (HONO concentrations from NO_2 heterogeneous reaction on the ground surface and photo-enhanced mechanisms, $HONO_{ground}$), dark red area (HONO concentrations from photolysis of atmospheric particulate NO_3^-, $HONO_{NO3\text{-}}$). In addition, orange area was the HONO production from the $f_{NH3,\ RH}$ factor on the aerosol surface ($HONO_{aerosol,\ NH3,\ RH}$).

Here, we simulated j_{NO3} (8.3×10^{-5}) by the factor of 5, a variation between −0.6% and 3.2% was proposed. The reasonable variation range implied the possibility of j_{NO3} change in our observed polluted days. Even so, NO_3^- photolysis was not that important in HONO formation during severely polluted days for the lack of solar radiation. HONO formation mostly came from NO_2 heterogeneous reactions. Heterogeneous reactions on the aerosol surface (including the effect of $f_{NH3,\ RH}$, subsequent expressions of heterogeneous reactions on the aerosol surface always include the $f_{NH3,\ RH}$ factor) and ground surface contributed to HONO of 68%, even contributed 91% in SPEs. After adding the "NO_2 heterogeneous reactions on aerosol surface and ground surface" mechanism to the base model simulations, about 76% of daily HONO and most HONO at noontime can be explained. The parameterization of NO_2 heterogeneous reactions was crucial to further quantify diurnal OH concentrations in model simulations during pollution episodes.

Environmental implications on haze pollution

Beijing is the typical megacity worldwide with condensed populations and buildings. Severe haze pollution generally occurs in autumn and winter. The pollution features include unfavorable diffusion and high humidity, which imply the potential capacity of local chemical conversions. RH and NH_3 concentrations can affect the properties of atmospheric aerosol (such as ALWC and aerosol pH) and atmospheric multiphase chemistry[60]. NH_3 is important in the atmosphere, which contributes to the formation of fine particles. NH_3-promoted NO_2 hydrolysis at the air-water surface, such as on the aerosol particles, is an important HONO formation pathway[35]. Abundant NH_3 concentrations and high RH in China cause aerosol pH values around 4–5, which were favorable for SO_2 oxidation by NO_2 and further HONO production[36,65]. Therefore, HONO concentrations increased partly caused by the developed haze and abundant NH_3 concentrations. In recent years, NH_3 emissions gradually increased or keep stable together with decreased NO_2 and SO_2 emissions[76,77]. In Beijing wintertime, NH_3 shows an increase of 59% on average from 2009 to 2016[78] and keeps stable till 2018[79]. Therefore, the role of NH_3 and HONO was more important than before.

After constraining the measured HONO concentrations to model, the OH concentrations were obtained (the following are simply expressed as OH concentrations). Diurnal average OH concentrations during 11:00–13:00 in PE1–4 were 1.3×10^6 cm^{-3}, 1.0×10^6 cm^{-3}, 0.9×10^6 cm^{-3}, 0.9×10^6 cm^{-3}, respectively, which were comparable to the levels measured in the winter polluted period of 2017 at a distance of one kilometer from our observation site of $1.5 \pm 0.9 \times 10^6$ cm^{-3} during 11:00–13:00[80] and in the other wintertime campaigns in urban areas[81–84]. HONO was the important species contributing to OH production in PEs (Supplementary Fig. 13)[14,15]. The reason is that the very low solar radiation during severely polluted days leads to low photolysis frequencies and low ozone concentrations[85]. We have summarized the contributions from HONO to OH in previous studies in Supplementary Table 7. Calculated by different methods (such as the general data analysis, Box-MCM, Box-RACM, WRF-Chem, CMAQ) in different types of locations, the contributions from HONO to OH are always significant, especially during higher polluted periods. The particulate matter growth during severe pollution episodes was generally underestimated, indicating the missing oxidation processes and/or oxidants in the current model simulations[10,11]. The OH concentrations from the base model included the contributions from O_3, HCHO, HONO (only one production pathway from ON and NO reaction), etc. The base model simulation explained 50% OH concentrations in PEs and 22% in SPEs. The added HONO formation pathways provided OH via HONO photolysis. After adding the HONO formation mechanisms of NO_2 heterogeneous reactions on the surfaces ($HONO_{hetero} = HONO_{aerosol} + HONO_{ground} + HONO_{aerosol,\ NH3,\ RH}$) in the model simulation, OH concentrations can be explained at 98% in PEs (Supplementary Fig. 11). Notably, $HONO_{hetero}$ contributed 48% OH concentrations in PEs and 78% OH concentrations during SPEs. With the development of haze pollution, the contribution from NO_2 heterogeneous conversion to HONO increased then the contribution to OH increased (Fig. 4). Take PE2 as an example, during 11:00 − 13:00 on the first day with $PM_{2.5}$ concentrations were 7 μg/m^3, $HONO_{hetero}$ contributed to HONO and OH of about 80% and 20%, respectively; during 11:00 − 13:00 in the last day with $PM_{2.5}$ concentrations were 252 μg/m^3, $HONO_{hetero}$ contributed to HONO and OH of about 93% and 79%, respectively. On the last day of each episode during 11:00 − 13:00, HONO and OH mostly came from the base model and $HONO_{hetero}$. Hence, only considering the $HONO_{hetero}$ in the base model simulations, OH concentrations can be well explained during pollution episodes and severe pollution episodes.

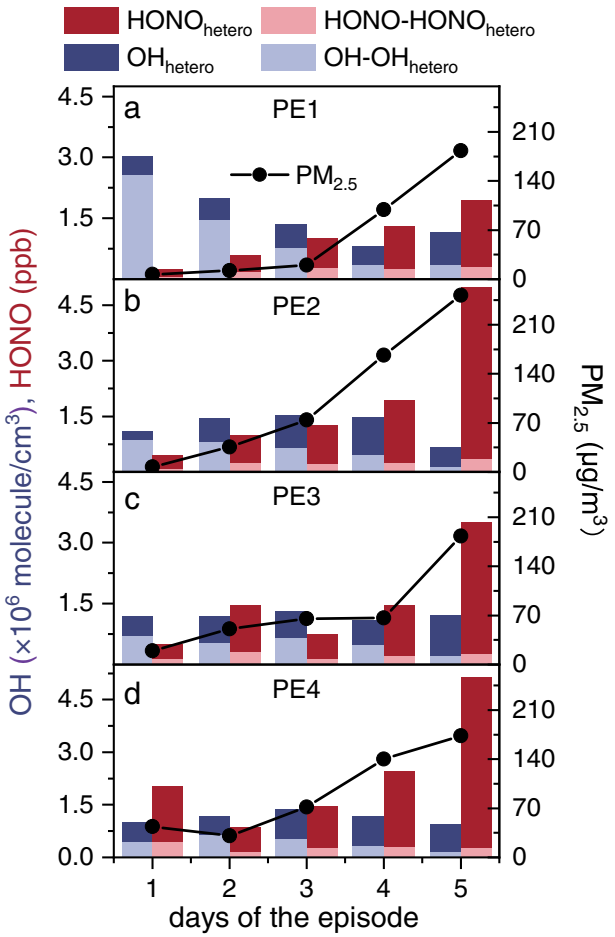

Fig. 4 The 11:00–13:00 average concentrations of OH, HONO, and $PM_{2.5}$ in polluted episodes. In (**a**) PE1, (**b**) PE2, (**c**) PE3, and (**d**) PE4, the dark color bar represents the HONO and OH concentrations change due to NO_2 heterogeneous reactions. The light color bar represents the other HONO and OH concentrations.

The OH concentrations increased by $HONO_{hetero}$ provided higher oxidizing capacity surroundings and activated chemical reactions in model simulations. Nitrogen oxidation ratio (NOR, $NO_3^-/(NO_3^- + NO_2)$) and sulfur oxidation ratio (SOR, $SO_4^{2-}/(SO_4^{2-} + SO_2)$) were 0.74 and 0.98, 0.43 and 0.74, 0.14 and 0.47 in SPEs, PEs, and clean days ($PM_{2.5} < 75$ μg/m^3), respectively. The high value of NOR and SOR during pollution episodes indicated the important secondary transformation.

NO_3^- can be produced by the gas-to-particle partition from HNO_3. The HNO_3 production rate mainly comes from $OH + NO_2$ and N_2O_5 hydrolysis ($P(HNO_3) = P(HNO_3)_{OH} + P(HNO_3)_{N2O5}$, Supplementary Note 5), which represents the upper limit of particle NO_3^- formation. In PEs, $P(HNO_3)_{OH}$ and $P(HNO_3)_{N2O5}$ were 0.68 ppb/h and 0.11 ppb/h in the daytime, and 0.06 ppb/h and 0.58 ppb/h in the nighttime. Nocturnal $P(HNO_3)_{N2O5}$ was much higher in PE2 (0.94 ppb/h), PE3 (0.44 ppb/h), and PE4 (0.58 ppb/h) than in PE1 (0.25 ppb/h), which confirmed the importance of heterogeneous reactions in PE2–4. $P(HNO_3)_{OH}$ dominated the diurnal HNO_3 formation during pollution episodes. $HONO_{hetero}$ can contribute to 0.9 μg/(m^3 h) NO_3^- production at most in PEs.

OH can also accelerate the SO_4^{2-} formation from SO_2 and OH gas-phase reaction. Harris et al. suggested that gas-phase oxidation is less important than aqueous-phase oxidation for SO_4^{2-} formation, gas-phase SO_4^{2-} formation accounted for 24% of observed SO_4^{2-}[86]. Based on the proportion, $HONO_{hetero}$ can contribute to 1.3 μg/m^3 SO_4^{2-} production at most by the gas-phase oxidation in PEs. Additionally, a recent study proposed that the SO_4^{2-} formation rate from NO_2 and SO_2 heterogeneous reaction on aerosols under winter haze conditions at aerosol pH of 5 was comparable to the levels of the missing sulfate source of 3 μg/(m^3 h)[10,36].

The accurate measurement or quantitative constraints of HONO were the key points to the understanding of the atmospheric oxidation capacity in model simulations during polluted periods. Our study proposed a new approach to elucidate the HONO budget on typical wintertime polluted days in the Chinese megacity, Beijing. Despite the large uncertainties (sensitivity tests in Supplementary Table 8 and Supplementary Discussion), the mechanisms were consistent with our field observation during four typical haze episodes. Besides, we validated these NO_2 heterogeneous conversion mechanisms (including the enhancement factor of $f_{NH3,\ RH}$) without adjustment in other wintertime polluted periods at the same site. Field observations were from January 2 to 20, 2019, and October 16 to 20, 2019, including four pollution episodes with $PM_{2.5}$ concentrations varied from 2 μg/m^3 to 574 μg/m^3 (Supplementary Table 9). After adding $HONO_{hetero}$ in model simulations, 32% OH concentrations during the observed periods and 89% OH concentrations during the severe pollution episodes were explained (RH > 70% and $PM_{2.5}$ >150 μg/m^3). And the OH concentrations simulated by adding parameterized NO_2 heterogeneous reactions were comparable to that by constraining observed HONO concentrations. Results demonstrated the validity and the potentially wide applicability of these NO_2 heterogeneous conversion mechanisms in urban Beijing during wintertime haze periods. Furthermore, NO_2, NH_3, and RH data can be obtained from emission inventory and the China Meteorological Administration's Satellite Data Broadcast System. Hence, $f_{NH3,\ RH}$ promoted NO_2 heterogeneous conversion mechanisms can be widely used in atmospheric model simulations, especially on highly polluted days.

In this work, the important role of NO_2 heterogeneous reactions in HONO formation was highlighted. Higher HONO produced more OH, and further more secondary inorganic aerosols formation. Reactions on $PM_{2.5}$ surfaces would accelerate again. All the above can create a phenomenon where haze pollution and HONO production mutually reinforces generation. To mitigate atmospheric pollution: ALWC is worthy of notice as the media of multiphase reactions; NH_3 emission control is proposed for its neutralization effect[87–89]. In urban cities, NH_3 and NO_X are largely released from combustion processes (power plants, vehicle emissions, coal-burning, etc)[90]. The combustion emission standard of NH_3 should be further optimized. In addition to the haze pollution in Beijing, the HONO formation mechanisms in this study are possibly widespread, accelerating the atmospheric nitrogen cycle and sulfur cycle. To better comprehend atmospheric pollution and human health, it's essential to measure or parameterize HONO.

METHODS

Experimental site and instrumentation

Field observation of HONO and other major air pollutants was conducted on the third floor of No.2 building at Institute of Chemistry, Chinese Academy of Sciences (ICCAS, 39°59′22.68″N, 116°19′21.58″E) in Beijing, which was a typical urban site and described in the previous studies in detail[45]. The instruments used in this study are listed in Supplementary Table 1. In this place, HONO was measured by a custom-made HONO analyzer, which has been used during previous observation periods[45,91]. The instrument's principle was consistent with the long path absorption photometer (LOPAP). The detection limit was 200 ppt. Response time was 13 min. Intercomparisons of commercial LOPAP and custom-made HONO analyzer proved the accuracy and reliability of our instrument[92]. In addition, a commercially

available monitor for gases and aerosols in ambient air (MARGA, 1 S, Metrohm Analytical B.V.) with a $PM_{2.5}$ inlet was used to quantify the water-soluble ions in $PM_{2.5}$ (Cl^-, NO_3^-, SO_4^{2-}, NH_4^+, Na^+, K^+, Mg^{2+}, Ca^{2+}) and precursor gases (NH_3, SO_2, HNO_3, and HCl). Meteorological parameters consisting of air temperature (T), relative humidity (RH), wind speed (WS), and wind direction (WD) were measured by a Vaisala weather transmitter (WXT520). The mixing ratios of NO, NO_2, and NO_X ($NO + NO_2$) were determined using a NO_X analyzer (Thermo Scientific, Model 42i) with the detection limit of 1 ppb. The chemiluminescence techniques would overestimate NO_2 concentrations by the interference of NO_y, so we corrected NO_2 concentrations as shown in Supplementary Note 1 and used it for discussion.

Another observation field was the Institute of Atmospheric Physics, Chinese Academy of Sciences (IAP, 39°58′54.91″N, 116°23′4.79″E), about 5 km southeast of the ICCAS site, which had similar surroundings of condensed population and heavy traffic. Aerosol surface area (S_{aero}) was measured by Scanning Mobility Particle Sizer (SMPS) with particle number size distributions from 14.5 nm to 710.5 nm. And photolysis frequencies (j_{O1D}, j_{HONO}, and j_{NO2}) were measured by photolysis spectrometers (PFS-100, Focused Photonics Inc.). The detailed information on S_{aero} and photolysis frequencies was described in previous studies[93,94]. Boundary layer height (BLH) was measured by a single-lens ceilometer, Vaisala CL51, Finland. Volatile organic compounds (VOCs) concentrations were gained from an automatic gas chromatograph system with a mass spectrometer and a flame ionization detector (GC-MS/FID)[95].

$PM_{2.5}$, CO, and O_3 were data from Wanliu monitoring station (got from the Beijing Municipal Biology Environment Bureau station), about 3 km southwest of the ICCAS measurement site. This site had similar surroundings to the above two sites.

Model description

Aerosol liquid water content (ALWC) and aerosol pH were derived by ISORROPIA-2 thermodynamic equilibrium model. Inorganic ions in $PM_{2.5}$ and gaseous precursors measured by the online ion chromatography system MARGA were constrained in the model. In the model, the forward mode was used for aerosols in the metastable conditions, and only data when 40% ≤RH < 95% were analyzed[59]. Comparison between observed and simulated inorganic ions in $PM_{2.5}$ and gaseous precursors showed consistency, which suggested the accuracy of model simulation[59,66]. Previous studies used the same method (ISORROPIA-2 model) to calculate the aerosol pH value during polluted days, and the calculated aerosol pH value (4.0–5.0)[66,71,96,97] was similar to ours.

HONO budget was explored by box model with MCM (master chemical mechanism version 3.3.1) mechanism. Box model is a zero-dimensional model, which is constrained by the profile of observed meteorological parameters and atmospheric pollutants concentrations. MCM is the most representative specific chemical mechanism. Each model species corresponds to an atmospheric compound and describes a series of chemical reactions in the atmosphere in detail. The summary of the constrained species in box model in this study is shown in Supplementary Table 2. The simulated interval was 1 h. Here, we only concentrated on pollution episodes with stagnant meteorological conditions. The most common source of HONO in model simulations was OH and NO homogeneous reaction. To improve the understanding of HONO, some HONO formation mechanisms were added to the simulation as exhibited in Table 1.

DATA AVAILABILITY

The data that support the findings of this study are available from the authors on reasonable request.

Received: 14 June 2022; Accepted: 15 May 2023;
Published online: 30 May 2023

REFERENCES

1. Li, X., Jin, L. & Kan, H. Air pollution: a global problem needs local fixes. *Nature* **570**, 437–439 (2019).
2. Shi, L. et al. A national cohort study (2000–2018) of long-term air pollution exposure and incident dementia in older adults in the United States. *Nat. Commun.* **12**, 6754 (2021).
3. Dedoussi, I. C., Eastham, S. D., Monier, E. & Barrett, S. R. H. Premature mortality related to United States cross-state air pollution. *Nature* **578**, 261–265 (2020).
4. Akimoto, H. Global air quality and pollution. *Science* **302**, 1716–1719 (2003).
5. Huang, R. et al. High secondary aerosol contribution to particulate pollution during haze events in China. *Nature* **514**, 218–222 (2014).
6. Womack, C. C. et al. An Odd Oxygen Framework for Wintertime Ammonium Nitrate Aerosol Pollution in Urban Areas: NOx and VOC Control as Mitigation Strategies. *Geophys. Res. Lett.* **46**, 4971–4979 (2019).
7. Franchin, A. et al. Airborne and ground-based observations of ammonium-nitrate-dominated aerosols in a shallow boundary layer during intense winter pollution episodes in northern Utah. *Atmos. Chem. Phys.* **18**, 17259–17276 (2018).
8. Tiwari, S. et al. Diurnal and seasonal variations of black carbon and $PM_{2.5}$ over New Delhi, India: Influence of meteorology. *Atmos. Res.* **125–126**, 50–62 (2013).
9. Kishore, N. et al. Long-term (2005–2012) measurements of near-surface air pollutants at an urban location in the Indo-Gangetic Basin. *J. Earth Syst. Sci.* **128**, 55 (2019).
10. Zheng, B. et al. Heterogeneous chemistry: a mechanism missing in current models to explain secondary inorganic aerosol formation during the January 2013 haze episode in North China. *Atmos. Chem. Phys.* **15**, 2031–2049 (2015).
11. Hofzumahaus, A. et al. Amplified trace gas removal in the troposphere. *Science* **324**, 1702–1704 (2009).
12. Kleffmann, J. et al. Daytime formation of nitrous acid: A major source of OH radicals in a forest. *Geophys. Res. Lett.* **32**, L05818 (2005).
13. Tan, Z. et al. Wintertime photochemistry in Beijing: Observations of ROx radical concentrations in the North China Plain during the BEST-ONE campaign. *Atmos. Chem. Phys.* **18**, 12391–12411 (2018).
14. Villena, G. et al. Nitrous acid (HONO) during polar spring in Barrow, Alaska: A net source of OH radicals? *J. Geophys. Res. Atmos.* **116**, D00R07 (2011).
15. Xue, C. et al. HONO budget and its role in nitrate formation in the rural North China plain. *Environ. Sci. Technol.* **54**, 11048–11057 (2020).
16. Lu, K. et al. Fast photochemistry in wintertime haze: Consequences for pollution mitigation strategies. *Environ. Sci. Technol.* **53**, 10676–10684 (2019).
17. Heard, D. E. et al. High levels of the hydroxyl radical in the winter urban troposphere. *Geophys. Res. Lett.* **31**, L18112 (2004).
18. Liu, Y. et al. A comprehensive model test of the HONO sources constrained to field measurements at rural North China Plain. *Environ. Sci. Technol.* **53**, 3517–3525 (2019).
19. Sommariva, R. et al. Enhanced wintertime oxidation of VOCs via sustained radical sources in the urban atmosphere. *Environ. Pollut.* **274**, 116563 (2021).
20. Atkinson, R. Atmospheric chemistry of VOCs and NOx. *Atmos. Environ.* **34**, 2063–2101 (2000).
21. Pagsberg, P., Bjergbakke, E., Ratajczak, E. & Sillesen, A. Kinetics of the gas phase reaction OH+NO(+M)→HONO(+M) and the determination of the UV absorption cross sections of HONO. *Chem. Phys. Lett.* **272**, 383–390 (1997).
22. Kurtenbach, R. et al. Investigations of emissions and heterogeneous formation of HONO in a road traffic tunnel. *Atmos. Environ.* **35**, 3385–3394 (2001).
23. Su, H. et al. Soil nitrite as a source of atmospheric HONO and OH Radicals. *Science* **333**, 1616–1618 (2011).
24. Gu, R. et al. Atmospheric nitrous acid (HONO) at a rural coastal site in North China: Seasonal variations and effects of biomass burning. *Atmos. Environ.* **229**, 117429 (2020).
25. Jenkin, M. E., Cox, R. A. & Williams, D. J. Laboratory studies of the kinetics of formation of nitrous acid from the thermal reaction of nitrogen dioxide and water vapour. *Atmos. Environ.* **22**, 487–498 (1988).
26. Ndour, M. et al. Photoenhanced uptake of NO_2 on mineral dust: Laboratory experiments and model simulations. *Geophys. Res. Lett.* **35**, L05812 (2008).
27. Notholt, J., Hjorth, J. & Raes, F. Formation of HNO_2 on aerosol surfaces during foggy periods in the presence of NO and NO_2. *Atmos. Environ., Part A. Gen. Top.* **26**, 211–217 (1992).
28. Stemmler, K., Ammann, M., Donders, C., Kleffmann, J. & George, C. Photosensitized reduction of nitrogen dioxide on humic acid as a source of nitrous acid. *Nature* **440**, 195–198 (2006).
29. Ye, C. et al. Rapid cycling of reactive nitrogen in the marine boundary layer. *Nature* **532**, 489–491 (2016).

30. Ye, C., Heard, D. E. & Whalley, L. K. Evaluation of Novel Routes for NOx Formation in Remote Regions. *Environ. Sci. Technol.* **51**, 7442–7449 (2017).
31. Ye, C., Zhang, N., Gao, H. & Zhou, X. Photolysis of Particulate Nitrate as a Source of HONO and NOx. *Environ. Sci. Technol.* **51**, 6849–6856 (2017).
32. Gen, M., Zhang, R., Huang, D. D., Li, Y. & Chan, C. K. Heterogeneous Oxidation of SO_2 in Sulfate Production during Nitrate Photolysis at 300 nm: Effect of pH, Relative Humidity, Irradiation Intensity, and the Presence of Organic Compounds. *Environ. Sci. Technol.* **53**, 8757–8766 (2019).
33. Stutz, J. et al. Relative humidity dependence of HONO chemistry in urban areas. *J. Geophys. Res. Atmos.* **109**, D03307 (2004).
34. Hao, N., Zhou, B., Chen, D. & Chen, L. Observations of nitrous acid and its relative humidity dependence in Shanghai. *J. Environ. Sci.* **18**, 910–915 (2006).
35. Li, L. et al. Formation of HONO from the NH_3-promoted hydrolysis of NO_2 dimers in the atmosphere. *Proc. Natl Acad. Sci. Usa.* **115**, 7236–7241 (2018).
36. Liu, T. & Abbatt, J. P. D. Oxidation of sulfur dioxide by nitrogen dioxide accelerated at the interface of deliquesced aerosol particles. *Nat. Chem.* **13**, 1173–1177 (2021).
37. Fu, X. et al. The significant contribution of HONO to secondary pollutants during a severe winter pollution event in southern China. *Atmos. Chem. Phys.* **19**, 1–14 (2019).
38. Liu, X. et al. Influences of relative humidity and particle chemical composition on aerosol scattering properties during the 2006 PRD campaign. *Atmos. Environ.* **42**, 1525–1536 (2008).
39. Li, Y. et al. Atmospheric nitrous acid (HONO) in an alternate process of haze pollution and ozone pollution in urban Beijing in summertime: Variations, sources and contribution to atmospheric photochemistry. *Atmos. Res.* **260**, 105689 (2021).
40. Guo, S. et al. Elucidating severe urban haze formation in China. *Proc. Natl Acad. Sci. Usa.* **111**, 17373–17378 (2014).
41. Zhang, D. Y., Liu, J. J. & Li, B. J. Tackling Air Pollution in China-What do We Learn from the Great Smog of 1950s in LONDON. *Sustainability* **6**, 5322–5338 (2014).
42. Zhang, R. et al. Formation of urban fine particulate matter. *Chem. Rev.* **115**, 3803–3855 (2015).
43. Cheng, Z. et al. Insights into extinction evolution during extreme low visibility events: Case study of Shanghai, China. *Sci. Total Environ.* **618**, 793–803 (2018).
44. Zhang, R., Khalizov, A., Wang, L., Hu, M. & Xu, W. Nucleation and growth of nanoparticles in the atmosphere. *Chem. Rev.* **112**, 1957–2011 (2012).
45. Tong, S. et al. Exploring the nitrous acid (HONO) formation mechanism in winter Beijing: direct emissions and heterogeneous production in urban and suburban areas. *Faraday Discuss.* **189**, 213–230 (2016).
46. Wang, J., Zhang, X., Guo, J., Wang, Z. & Zhang, M. Observation of nitrous acid (HONO) in Beijing, China: Seasonal variation, nocturnal formation and daytime budget. *Sci. Total Environ.* **587–588**, 350–359 (2017).
47. Tong, S. R. et al. Comparisons of measured nitrous acid (HONO) concentrations in a pollution period at urban and suburban Beijing, in autumn of 2014. *Sci. China-Chem.* **58**, 1393–1402 (2015).
48. Hao, Q., Jiang, N., Zhang, R., Yang, L. & Li, S. Characteristics, sources, and reactions of nitrous acid during winter at an urban site in the Central Plains Economic Region in China. *Atmos. Chem. Phys.* **20**, 7087–7102 (2020).
49. Zhang, X. et al. The Levels and Sources of Nitrous Acid (HONO) in Winter of Beijing and Sanmenxia. *J. Geophys. Res. Atmos.* **127**, e2021JD036278 (2022).
50. Huang, R. et al. Concentration and sources of atmospheric nitrous acid (HONO) at an urban site in Western China. *Sci. Total Environ.* **593–594**, 165–172 (2017).
51. Zhang, W. et al. Variations and sources of nitrous acid (HONO) during a severe pollution episode in Beijing in winter 2016. *Sci. Total Environ.* **648**, 253–262 (2019).
52. Jia, C. et al. Pollution characteristics and potential sources of nitrous acid (HONO) in early autumn 2018 of Beijing. *Sci. Total Environ.* **735**, 139317 (2020).
53. Xu, Z. et al. Nitrous acid (HONO) in a polluted subtropical atmosphere: Seasonal variability, direct vehicle emissions and heterogeneous production at ground surface. *Atmos. Environ.* **106**, 100–109 (2015).
54. Yun, H. et al. Nitrous acid in a street canyon environment: Sources and contributions to local oxidation capacity. *Atmos. Environ.* **167**, 223–234 (2017).
55. Xue, C. et al. Atmospheric measurements at Mt. Tai – Part II: HONO budget and radical (RO_3+NO_3) chemistry in the lower boundary layer. *Atmos. Chem. Phys.* **22**, 1035–1057 (2022).
56. Liu, Y. et al. Semi-quantitative understanding of source contribution to nitrous acid (HONO) based on 1 year of continuous observation at the SORPES station in eastern China. *Atmos. Chem. Phys.* **19**, 13289–13308 (2019).
57. Tan, Z. F. et al. Radical chemistry at a rural site (Wangdu) in the North China Plain: observation and model calculations of OH, HO_2 and RO_2 radicals. *Atmos. Chem. Phys.* **17**, 663–690 (2017).
58. Tie, X. X. et al. Ozone enhancement due to the photodissociation of nitrous acid in eastern China. *Atmos. Chem. Phys.* **19**, 11267–11278 (2019).
59. Guo, H. et al. Fine particle pH and the partitioning of nitric acid during winter in the northeastern United States. *J. Geophys. Res. Atmos.* **121**, 10355–10376 (2016).
60. Zheng, G. et al. Multiphase buffer theory explains contrasts in atmospheric aerosol acidity. *Science* **369**, 1374–1377 (2020).
61. Saliba, N. A., Yang, H. & Finlayson-Pitts, B. J. Reaction of gaseous nitric oxide with nitric acid on silica surfaces in the presence of water at room temperature. *J. Phys. Chem. A* **105**, 10339–10346 (2001).
62. Goodman, A. L., Bernard, E. T. & Grassian, V. H. Spectroscopic study of nitric acid and water adsorption on oxide particles: Enhanced nitric acid uptake kinetics in the presence of adsorbed water. *J. Phys. Chem. A* **105**, 6443–6457 (2001).
63. Yang, S. et al. Chemistry of new particle formation and growth events during wintertime in suburban area of Beijing: Insights from highly polluted atmosphere. *Atmos. Res.* **255**, 105553 (2021).
64. Chen, T. et al. Enhancement of aqueous sulfate formation by the coexistence of NO_2/NH_3 under high ionic strengths in aerosol water. *Environ. Pollut.* **252**, 236–244 (2019).
65. Cheng, Y. et al. Reactive nitrogen chemistry in aerosol water as a source of sulfate during haze events in China. *Sci. Adv.* **2**, e1601530 (2016).
66. Ding, J. et al. Aerosol pH and its driving factors in Beijing. *Atmos. Chem. Phys.* **19**, 7939–7954 (2019).
67. Freedman, M. A. Phase separation in organic aerosol. *Chem. Soc. Rev.* **46**, 7694–7705 (2017).
68. Kinugawa, T. et al. Conversion of gaseous nitrogen dioxide to nitrate and nitrite on aqueous surfactants. *Phys. Chem. Chem. Phys.* **13**, 5144–5149 (2011).
69. Li, L., Hoffmann, M. R. & Colussi, A. J. Role of Nitrogen Dioxide in the Production of Sulfate during Chinese Haze-Aerosol Episodes. *Environ. Sci. Technol.* **52**, 2686–2693 (2018).
70. Wang, J. et al. Fast sulfate formation from oxidation of SO_2 by NO_2 and HONO observed in Beijing haze. *Nat. Commun.* **11**, 2844 (2020).
71. Song, S. et al. Fine-particle pH for Beijing winter haze as inferred from different thermodynamic equilibrium models. *Atmos. Chem. Phys.* **18**, 7423–7438 (2018).
72. Liu, M. X. et al. Fine particle pH during severe haze episodes in northern China. *Geophys. Res. Lett.* **44**, 5213–5221 (2017).
73. Ge, S. et al. Abundant NH_3 in China Enhances Atmospheric HONO Production by Promoting the Heterogeneous Reaction of SO_2 with NO_2. *Environ. Sci. Technol.* **53**, 14339–14347 (2019).
74. Wang, G. et al. Persistent sulfate formation from London Fog to Chinese haze. *Proc. Natl Acad. Sci. USA* **113**, 13630–13635 (2016).
75. Wang, G. Y. et al. Barrierless HONO and HOS(O)(2)-NO_2 Formation via NH_3-Promoted Oxidation of SO_2 by NO_2. *J. Phys. Chem. A* **125**, 2666–2672 (2021).
76. Kang, Y. et al. High-resolution ammonia emissions inventories in China from 1980 to 2012. *Atmos. Chem. Phys.* **16**, 2043–2058 (2016).
77. Liu, X. J. et al. Environmental impacts of nitrogen emissions in China and the role of policies in emission reduction. *Philos. Trans. R. Soc., A* **378**, 20190324 (2020).
78. Meng, Z. et al. Changes in ammonia and its effects on $PM_{2.5}$ chemical property in three winter seasons in Beijing, China. *Sci. Total Environ.* **749**, 142208 (2020).
79. Wen, Z. et al. Winter air quality improvement in Beijing by clean air actions from 2014 to 2018. *Atmos. Res.* **259**, 105674 (2021).
80. Ma, X. et al. Winter photochemistry in Beijing: Observation and model simulation of OH and HO_2 radicals at an urban site. *Sci. Total Environ.* **685**, 85–95 (2019).
81. Ren, X. et al. Behavior of OH and HO_2 in the winter atmosphere in New York City. *Atmos. Environ.* **40**, 252–263 (2006).
82. Kanaya, Y. et al. Urban photochemistry in central Tokyo: 1. Observed and modeled OH and HO_2 radical concentrations during the winter and summer of 2004. *J. Geophys. Res. Atmos.* **112**, D21312 (2007).
83. Slater, E. J. et al. Elevated levels of OH observed in haze events during wintertime in central Beijing. *Atmos. Chem. Phys.* **20**, 14847–14871 (2020).
84. Emmerson, K. M. et al. Urban atmospheric chemistry during the PUMA campaign 1: Comparison of modelled OH and HO_2 concentrations with measurements. *J. Atmos. Chem.* **52**, 143–164 (2005).
85. Alicke, B. et al. OH formation by HONO photolysis during the BERLIOZ experiment. *J. Geophys. Res. Atmos.* **108**, 8247 (2003).
86. Harris, E. et al. Enhanced role of transition metal ion catalysis during in-cloud oxidation of SO_2. *Science* **340**, 727–730 (2013).
87. Liu, M. et al. Ammonia emission control in China would mitigate haze pollution and nitrogen deposition, but worsen acid rain. *Proc. Natl. Acad. Sci. USA* **116**, 7760–7765 (2019).
88. Liu, Z. et al. The nonlinear response of fine particulate matter pollution to ammonia emission reductions in North China. *Environ. Res. Lett.* **16**, 034014 (2021).
89. Zhai, S. et al. Control of particulate nitrate air pollution in China. *Nat. Geosci.* **14**, 389–395 (2021).
90. Qiu, C. & Zhang, R. Multiphase chemistry of atmospheric amines. *Phys. Chem. Chem. Phys.* **15**, 5738–5752 (2013).
91. Zhang, W. et al. Different HONO sources for three layers at the urban area of Beijing. *Environ. Sci. Technol.* **54**, 12870–12880 (2020).
92. Hou, S., Tong, S., Ge, M. & An, J. Comparison of atmospheric nitrous acid during severe haze and clean periods in Beijing, China. *Atmos. Environ.* **124**, 199–206 (2016).

93. Liu, Z., Hu, B., Zhang, J., Yu, Y. & Wang, Y. Characteristics of aerosol size distributions and chemical compositions during wintertime pollution episodes in Beijing. *Atmos. Res.* **168**, 1–12 (2016).
94. Hu, B. et al. Quantification of the impact of aerosol on broadband solar radiation in North China. *Sci. Rep.* **7**, 44851 (2017).
95. Wang, M. et al. Development and validation of a cryogen-free automatic gas chromatograph system (GC-MS/FID) for online measurements of volatile organic compounds. *Anal. Methods* **6**, 9424–9434 (2014).
96. Shi, G. et al. pH of aerosols in a polluted atmosphere: source contributions to highly acidic aerosol. *Environ. Sci. Technol.* **51**, 4289–4296 (2017).
97. Tan, T. et al. New insight into $PM_{2.5}$ pollution patterns in Beijing based on one-year measurement of chemical compositions. *Sci. Total Environ.* **621**, 734–743 (2018).
98. Zhou, X. et al. Nitric acid photolysis on surfaces in low-NOx environments: Significant atmospheric implications. *Geophys. Res. Lett.* **30**, 2217 (2003).
99. Harrison, R. M., Peak, J. D. & Collins, G. M. Tropospheric cycle of nitrous acid. *J. Geophys. Res. Atmos.* **101**, 14429–14439 (1996).

ACKNOWLEDGEMENTS

This work was supported by the National Natural Science Foundation of China (Contract No. 41830106, 42022039), Beijing National Laboratory for Molecular Sciences (BNLMS-CXXM-202011), Youth Innovation Promotion Association of Chinese Academy of Sciences (Y2021013). We thank Prof. Qifan Liu (Air Quality Processes Research Section, Environment and Climate Change Canada) and Prof. John Liggio (Air Quality Processes Research Section, Environment and Climate Change Canada) for helpful comments and improvement on the manuscript.

AUTHOR CONTRIBUTIONS

X.Z. and S.T. designed the research; X.Z., S.T., G.T., B.H., Z.L., L.W., P.Z., Y.P., and M.G. performed the research; X.Z., S.T., C.J., P.Z., and M.G. contributed new reagents/analytic tools; X.Z., S.T., C.J., W.Z., and Z.W. analyzed data; X.Z. and S.T. wrote the paper.

COMPETING INTERESTS

The authors declare no competing interests.

ADDITIONAL INFORMATION

Supplementary information The online version contains supplementary material available at https://doi.org/10.1038/s41612-023-00371-w.

Correspondence and requests for materials should be addressed to Shengrui Tong or Maofa Ge.

Reprints and permission information is available at http://www.nature.com/reprints

Publisher's note Springer Nature remains neutral with regard to jurisdictional claims in published maps and institutional affiliations.